

Photon states in one-dimensional photonic crystals based on porous silicon multilayers

C. J. Oton , L. Dal Negro, P. Bettotti, L. Pancheri, Z. Gaburro, L. Pavesi

INFM and Department of Physics,

University of Trento, via Sommarive 14, Povo (TN), Italy.

22-May-02

Porous silicon (PS) multilayers allow a wide tunability of the refractive index and are therefore good candidates to fabricate one-dimensional photonic crystals. The emission properties of PS and Er-doped PS photonic crystals are strongly modified with respect to homogeneous PS structures: strong luminescence narrowing, intensity enhancement and emission directionality have been shown. In addition, the photon propagation in one-dimensional complex systems, such as Fibonacci quasicrystals made by porous silicon multilayers, shows a variety of interesting phenomena among which the appearance of localized and critical states. Photonic Bloch oscillations in time domain have never been observed; here we discuss a PS multilayer structure that should allow their observation.

1. INTRODUCTION

In recent years, an increasing effort has been dedicated to photonic structures because of their wide application in the control of the emission, propagation, and detection of light [1]. Photonic crystals, waveguides, microcavities, and filters are only a few examples of such photonic structures. Recently we focused on one-dimensional photonic structures based on porous silicon (PS). PS is very easy to grow and allows a wide tunability of its dielectric properties. This fact allows realizing very interesting planar devices to observe a large variety of phenomena associated with the photon states in 1D photonic crystals.

In this paper we report on some new perspectives where 1D photonic crystals based on PS can play an interesting role in order to unfold some interesting physical phenomena. Some experiments and new theoretical suggestions will be presented. Section 2 describes very shortly how PS dielectric multilayers can be fabricated. Section 3 introduces the method used to simulate the photonic states in PS multilayers. Section 4 presents some experimental data as well as simulations of 1D photonic crystals with a defect based on PS. Here, the influence of the 1D photonic structure on the emission of both PS and Er-doped PS is discussed. Section 5 is about complex photonic systems based on PS. As a prototype 1D Fibonacci quasicrystals are presented. Transmission experiments are compared with simulations and the character of the optical photon modes in Fibonacci quasicrystals is analyzed. Section 6 approaches the problem of photonic Bloch oscillations and we suggest a PS structure where it is possible to observe them. We purposely omit to review our previous works, where we refer the reader.

2. FABRICATION OF POROUS SILICON MULTILAYERS

Porous silicon (PS) is formed by electrochemical etching of doped Si in an HF based electrolyte [2]. Many review papers on PS formation and properties have been published [3]. Here it is important to

point out that the structure of PS is influenced by several parameters: HF content in the electrolyte, Si doping and current density. In particular, the Si doping influences the diameter of the pores: nanopores of about 1-3 nm size are obtained in lightly doped p-type Si, while larger pores (mesopores) of 5-20 nm size are obtained in heavily doped Si. The actual pore size is controlled by the current density: the higher the current the larger the sizes are. For both doping densities, the typical structure sizes are much smaller than the wavelength of light in the visible range. Hence PS can be approximated by an effective medium, whose index of refraction n has an intermediate value between that of Si and of air. A simple estimation of the effective dielectric constant $\varepsilon_{eff}=n^2$ of PS can be obtained by the Bruggeman effective medium theory [4,5]:

$$f \frac{\varepsilon - \varepsilon_{eff}}{\varepsilon + 2\varepsilon_{eff}} + (1-f) \frac{\varepsilon_M - \varepsilon_{eff}}{\varepsilon_M + 2\varepsilon_{eff}} = 0 \quad (1),$$

where f is the volumetric fraction of Si in PS –the porosity $\wp = (1-f)$ – and ε , ε_M are the dielectric functions of Si and of the embedding medium (air). The value of \wp is determined also by the pore sizes.

In order to fabricate 1D photonic structures, such as those provided by dielectric multilayers, a controlled variation of n in one direction is needed. This is possible by using PS [4]. As n depends on \wp , which in turn depends on the current density, one can modulate the current during the etch to profile $n(z)$. Moreover, as the etch occurs only at the pore tips, a change in the current density does not modify the already etched layers (see fig. 1). This fact allows the fabrication of a PS sample with any desired n profile; *i. e.* 1D photonic structures can be grown by using PS. A critical issue is the range of n achievable: with lightly doped Si the range is quite small (approximately from $n=1.4$ to 1.7) since only high porosities are attainable; with heavily doped Si much lower porosities can be obtained too, therefore n can be varied from about 1.4 to 2.4 [4]. The drawback of using heavily doped Si is that the luminescence is very weak, but this is not a problem for the fabrication of passive optical devices. Examples of multilayers obtained by using PS are reported in ref. [4, 6].

3. SIMULATION OF POROUS SILICON MULTILAYERS

To understand the photon states and their propagation in PS multilayers, we calculated their reflectance and transmittance spectra by means of a simple transfer-matrix approach [7]. Assuming plane waves, the electric (E_l) and magnetic (B_l) field at the left interface of a dielectric layer can be related to E_r and B_r at the right interface of the same layer through a simple matrix relation:

$$\begin{pmatrix} E_l \\ B_l \end{pmatrix} = M \begin{pmatrix} E_r \\ B_r \end{pmatrix} = \begin{pmatrix} \cos \delta & i \sin \delta / \gamma \\ i \gamma \sin \delta & \cos \delta \end{pmatrix} \begin{pmatrix} E_r \\ B_r \end{pmatrix} \quad (2),$$

where $\delta = k_0 n d$ is the phase change, k_0 is the wave number of the light in vacuum, n is the refractive index of the layer, d is the thickness of the layer, and γ is the inverse of the light velocity across the layer. From the continuity requirements of the parallel components of E and B and by simple matrix multiplication, one can construct the transfer matrix M relating the input with the output fields for a system of N layers:

$$\begin{pmatrix} E_0 \\ B_0 \end{pmatrix} = M_1 M_2 \dots M_N \begin{pmatrix} E_N \\ B_N \end{pmatrix} = M \begin{pmatrix} E_N \\ B_N \end{pmatrix} \quad (3),$$

where M_i is the transfer-matrix of the i^{th} layer (eq. 2), E_0 and B_0 the fields at the first interface, and E_N and B_N the fields at the last interface. The total complex transmission $t(\omega)$ and reflection $r(\omega)$ coefficients can be obtained from M by assuming an incident white light beam of intensity normalized to one coming from the left and no light coming from the right. With these boundary conditions we get the following equations [7]:

$$\begin{aligned} r(\omega) &= \frac{\gamma_0 m_{11} + \gamma_0 \gamma_s m_{12} - m_{21} - \gamma_s m_{22}}{\gamma_0 m_{11} + \gamma_0 \gamma_s m_{12} + m_{21} + \gamma_s m_{22}} \\ t(\omega) &= \frac{2\gamma_0}{\gamma_0 m_{11} + \gamma_0 \gamma_s m_{12} + m_{21} + \gamma_s m_{22}} \end{aligned} \quad (4)$$

where $m_{\alpha\beta}$ are the elements of M , and γ_0 and γ_s the inverse of the velocity of light in the input (for air $\gamma_0=c^{-1}$) and the output media, respectively. Since PS multilayers are grown on top of a Si substrate, the output media is assumed to be the Si substrate.

$t(\omega)$ contains information on both the amplitude and the phase of the transmitted light. The dispersion properties of light propagating through the PS multilayers can be retrieved from the phase of $t(\omega)$ [8]. Since finite structures are non-periodic, we define an effective wavevector k_{eff} by $\varphi = k_{eff} d_{tot}$, being φ the phase of the complex transmission coefficient and d_{tot} the total thickness of the PS multilayer. Given $k_{eff}(\omega)$, the photon mode density $\rho(\omega)$ and the group velocity $v_g(\omega)$ are calculated with the following relations [8]:

$$\begin{aligned}\rho(\omega) &= \frac{dk_{eff}}{d\omega} \\ v_g(\omega) &= \frac{1}{\rho(\omega)}\end{aligned}\tag{5}$$

It is possible to compute the electric field distribution *inside* the sample for any frequency [9]. Starting from $r(\omega)$ (eq. 4), the electric field on the k^{th} interface can be expressed as:

$$E(z^k, \omega) = (1 + r(\omega))m_{22}^k - \gamma_0(1 - r(\omega))m_{12}^k\tag{6}$$

where $m_{\alpha\beta}^k$ are the elements of a transfer matrix obtained as in eq. 3 by multiplication of the various M_i from the first to the k^{th} layer. $E(z, \omega)$ represents the scattering states of the structure. With $E(z, \omega)$, the time evolution of a light pulse propagating through the sample can be simulated by a Fourier transformation:

$$E(z, t) \propto \int E(z, \omega)X(\omega)e^{i\omega t} d\omega\tag{7}$$

being $X(\omega)$ the frequency profile of the incoming light pulse.

4. 1D PHOTONIC CRYSTAL WITH A DEFECT

The simplest 1D photonic crystal consists of a periodic sequence of two layers with two different n and the same nd . It is usually called Distributed Bragg Reflector (DBR) since for a wavelength range around $\lambda = 4nd$ the structure reflects most of the incoming light. This wavelength range is named stop-band. High reflection is a consequence of the fact that light cannot propagate with a \mathbf{k} vector in the stop-band since it is a forbidden quantum state. In analogy to the electronic case, the stop-band is also called a *photonic band-gap* and the DBR a 1D photonic crystal [1]. With the same nomenclature, a Fabry-Perot resonator or microcavity, where a layer is surrounded by two equal DBR, can be described as a defect in a 1D photonic crystal. In fact, if the central layer has $nd = \lambda/2$ and the DBRs have $nd = \lambda/4$, a localized state appears in the middle of the photonic band-gap. The presence of the defect can be observed in the reflectance spectrum as a narrow transmittance peak in the stop-band. Using PS, such structures can be easily fabricated [4, 10]. Figure 2 reports a comparison between simulated and experimental reflectance spectra for a 1D photonic crystal with a defect made by a PS microcavity centered at 700 nm sandwiched between two 6-period DBRs. The good agreement between theory and experiment shows both the mastering of the growth process and the correctness of the theoretical approach. Figure 3 shows calculations of $\rho(\omega)$ and $v_g(\omega)$ of this defected 1D photonic crystal. A low $\rho(\omega)$ in the photonic band gap with a narrow intense peak due to the mode localized on the defect is observed. $v_g(\omega)$ becomes superluminal in the photonic band gap due to Bragg interference [11], while $v_g(\omega)$ at the defect becomes very low; a time-resolved transmission experiment tuned to the defect wavelength should reveal dramatic effects on pulse propagation. Figure 4 shows the scattering states map $E(z, \omega)$. A strong field enhancement is observed at the defect energy and position: energy gets accumulated on the defect and the electric field becomes higher than the incoming field. The enhancement factor becomes near 100 in the center of the defect. This phenomenon can be exploited in photonic active devices, because, through Fermi's golden rule, the localized mode increases strongly the emission (and absorption) properties of the active layer.

4.1 MODIFICATION OF PS EMISSION

The emission properties of the 1D photonic crystal with defect previously described, are shown in fig. 5 [10]. A narrowing and enhancement of the photoluminescence with respect to the usual broad-emission of PS is observed due to the field enhancement at the defect (Fig. 5a). The emission is also highly directional because the mode density is strongly dependent not only on the modulus of the \mathbf{k} vector but also on its direction. A very good correspondence between the emission peak and the reflection dip is observed (Fig. 5b).

4.2 MODIFICATION OF ERBIUM EMISSION IN PS

The same effect can be observed when optically active centers are inserted in the 1D photonic crystal. We used Er^{3+} ions as active centers by impregnation of PS samples in order to access the 1.53-1.55 μm window, which is important for optical communications [12,13].

Er^{3+} ions are electro-migrated into PS by applying a cathodic polarization to PS samples immersed in ErCl_3 /ethanol saturated solution (we applied a current of 140 $\mu\text{A}/\text{cm}^2$). In order to oxidize PS and, hence, to activate the Er luminescence, a thermal treatment at 1100°C for 30 seconds in air was performed [12]. As we aim to place the Er ions in a 1D photonic crystal with a defect resonant with the Er emission, the oxidation of PS should be considered when the structure is designed [13]. A typical blue-shift of 170 nm at 1.5 μm is observed between the reflectance of PS multilayers before and after the oxidation. In fact, oxidation partially replaces Si with SiO_2 in PS, which means that in eq. 1, n of Si should be replaced by that of SiO_2 .

After a careful design, 1D photonic crystals with defect resonant with the Er emission can be obtained; an example is reported in fig. 6. Figure 6 reports: i) the luminescence spectrum of an Er-doped PS layer (dashed line) which is characterized by a wide structured peak at 1533 nm; ii) the luminescence of an Er-doped 1D photonic crystals with a resonant defect (line and triangles)

collected along the 1D axis; iii) the calculated reflectance spectrum for this defect (line and triangles); and iv) the same two quantities for a collecting angle of 23° with respect to the 1D axis (line and circles). The Er emission is changed when Er is placed into the 1D photonic crystals: a narrowed, symmetric and enhanced emission is observed. All these features are clear signatures of the resonant coupling of the Er with the defect in the 1D photonic crystal. This fact is also confirmed by the observation of the emission from the Er doped sample from an angle different than the sample normal. Both experiment and simulation show blue-shifts of the emission peak and reflectance dip. As this system is not optimized yet, we measured also some luminescence at 1531 nm due to the presence of Er oxide on the sample surface.

5. COMPLEX STRUCTURES

Complex photonic structures are dielectric structures where n fluctuates over length scales comparable with λ . If n fluctuates randomly in space the resulting structures are referred to as random photonic structures. These are indeed good examples of a complex structure. In the last 15 years, many other complex photonic structures have been discovered: e.g. the fractal and quasiperiodic structures, where the n variations are neither random nor periodic, even if deterministically generated. Many peculiar and fascinating phenomena, such as fracton modes [14] (localized photons in fractals), self-similar wave functions [15], critical diffusion [16], marginal diffusion [17], are directly related to the wave propagation in self-similar (fractal) media. Here we focus on spatial field localization (field enhancement) and light localization of photons, which not only characterize finite size periodic structures (see previous section) but have been theoretically predicted also for *aperiodic fractal* structures such as those realized with the Fibonacci or Cantor generating rule [18]. Field localization and enhancement in quasiperiodic structures are suggesting many possible applications for optical devices such as band-edge lasing [19], efficient nonlinear filters [20], bistability [21], switching [22], and gap-solitons.

An important class of deterministic aperiodic structures is represented by the Fibonacci quasicrystals [23, 24, 25]. A 1D Fibonacci quasicrystal can be constructed as a stack of two layers A and B distributed as the binary quasiperiodic Fibonacci sequence $S_{j+1}=\{S_{j-1}S_j\}$ for $j \geq 1$; with $S_0=\{B\}$ and $S_1=\{A\}$. $S_2=\{BA\}$, $S_3=\{ABA\}$, $S_4=\{BAABA\}$, etc. Transmission spectra of quasiperiodic structures possess a rich fractal nature and very narrow resonance peaks are separated by forbidden frequency regions, called “pseudo-band gaps”, despite the global structure is not periodic. Any substitutional sequence is characterized by the nature of its Fourier spectrum. Figure 7 shows the comparison among the Fourier spectra of a periodic, a random and a Fibonacci structure. The periodic structure shows a single peak due to the periodicity in its sequence. The random structure shows a white background because of the lack of periodicity. Finally, the Fibonacci structure represents an intermediate situation: it reveals strong and narrow peaks due to short-range order but also many weak peaks along the whole frequency spectrum as a trace for the global lack of periodicity.

By using PS, we have grown Fibonacci quasicrystals up to $j = 12$, *i. e.* up to 233 layers. Starting from a p^+ -type doped Si wafer, we have chosen for B = S_0 a 165 nm thick layer with $\phi = 66\%$ and for A = S_1 a 110nm thick layer with $\phi = 45\%$. The total thickness was approximately 30 μm . Figure 8 reports the transmission spectrum of the Fibonacci structure measured by a Fourier Transform Infrared Spectrometer (FTIR) together with its transfer-matrix simulation. Some degrees of disorder have to be considered in the simulation. In fact, during the electrochemical attack the etching velocity decreases, progressively reducing the actual layer thickness and increasing their porosities [26]. For this, we let the thickness of the A-layers to vary linearly up to a maximum 6% of its initial value; the thickness of the B-layers has been linearly varied of less than 1%, while the two porosities have been varied up to a 10% of their initial values. In addition we considered the effect of the FTIR finite beam width ($\approx 4\text{mm}$) on the sample. Because of the unavoidable sample lateral inhomogeneities, the measured transmission is an average over different sample contributions.

Considering a lateral sample inhomogeneity within a 1% of the nominal thickness value, we obtained a reasonable agreement with the measured transmission spectrum, as shown in fig. 8. This agreement substantiates the following analysis, which is based on this model structure.

To understand the physics of this Fibonacci quasicrystal, we performed a scattering states simulation of the field intensities inside it for frequencies near the large pseudo-gap at 5000 cm^{-1} (fig. 9). Many pseudo-band gaps separated by narrow transmission states with field enhancement are visible. Field enhancement is addressed in fig. 10, where the electric field intensity at four different frequencies is reported. The two upper profiles (5220 cm^{-1} and 5350 cm^{-1}) refer to the band-edge resonances near the pseudo-gap. Their field is enhanced by a factor of 16, while the local density of states is very high. Field enhancement is also present for the quasi-localized (also called weakly localized) states far from the band-edges, as those reported in the two bottom panels of fig. 10. Here dispersive effects due to the band-edges are completely absent. Indeed the field profiles for band-edge modes and these modes show very different envelopes, suggesting a completely distinct physical nature. These modes are clearly not Bloch states of the structure nor exponentially localized ones, suggesting the critical states interpretation with self-similarity [27]. The fractal nature of these light states is indeed clearly distinguishable in a Fibonacci structure of higher order, where a more specialized scaling analysis can be performed.

Time-resolved coherent transmission experiment, resonantly performed by exciting different modes, could be performed to address experimentally the question of the nature of these modes. A preliminary account of this work is reported in [28]. We found that 100 fs long light pulses resonant with the band-edge modes at 5000 cm^{-1} are extremely delayed and stretched on a picosecond time scale after transmission through the Fibonacci quasicrystal of fig. 8. This is a consequence of the strongly reduced group velocity for frequencies close to the band edge of a quasicrystal. Coherent beating among different modes are also observed.

6. PHOTONIC BLOCH OSCILLATIONS

A sufficiently large electric bias applied to a semiconductor superlattice causes the formation of the so-called Wannier-Stark ladder (WSL), where localized quantum well states replace the extended miniband state in the superlattice energy spectrum [29]. In 1928, Bloch predicted that an electronic wave packet propagating through WSL would oscillate periodically (Bloch oscillations) [30]. Electronic Bloch oscillations have been observed experimentally in 1992 by Feldmann *et al* [31]. By analogy, photonic Bloch oscillations (PBO) could exist also in carefully designed photonic structures. The challenge for PBO is the realization of a WSL. Many ideas have been recently proposed such as graded lateral confinement [9], thermal gradient [32], curved waveguides [33], *etc.* PBO have been recently observed in an array of waveguides [34], where the PBO were not resolved in time but in space. In ref. [35], a structure of interacting defects based on $\text{Al}_{1-x}\text{Ga}_x\text{As}$ is proposed to observe time-resolved PBO. Here we propose to use a 1D photonic crystal with a series of interacting defects based on PS to observe PBO.

The structure is based on weakly coupled microcavities [36]. The starting structure is based on PS multilayers and is tailored to the 1.4 μm wavelength region. It is formed by a series of DBR composed by two layers of thickness 46 and 64 nm, of porosities 44% and 66%, *i. e.* $n=2.2$ or 1.6. After each $4\frac{1}{2}$ -period of the DBR, a $\lambda/2$ thick with 66% porosity spacer layer is inserted. A total of 10 spacer layers, *i. e.* 10 weakly coupled microcavity, forms the structure. Its photon mode spectrum is characterized by a miniband of optical modes, which is formed at the center of the photonic band-gap of the DBR due to the coupling of the various microcavities. This structure is the photonic analogous of an electronic superlattice. If a 20% gradient in the layer thicknesses is applied –see fig. 11– the microcavity coupling vanishes and a photonic WSL forms. Figure 12 shows the scattering states of the structure, where localized modes due to the WSL can be observed. To evidence that PBO can be observed, the temporal response of the structure to a coherent pulse is simulated with eq. 7, where $X(\omega)$ is a gaussian pulse centered at 6970 cm^{-1} and 100 cm^{-1}

wide (FWHM). The pulse propagation through the structure is reported in fig. 13, where PBO are visible. When the photon pulse reaches the structure ends, it is back reflected and partially transmitted. The light intensity escaping from the sample is plotted in fig. 14: PBO are evident both in reflection and in transmission. Their period τ is about 260 fs. Bloch proposed a simple semi classical approach to calculate τ for electron oscillations [30]:

$$\tau = \frac{h}{eF\Lambda} \quad (8),$$

where h and e are the Planck's constant and the electronic charge, F is the electric field, and Λ is the period of the superlattice. The equivalent formula for photons, when energy is given in cm^{-1} , would be:

$$\tau = \frac{1}{c \left(\frac{\Delta E}{d_{tot}} \right) \Lambda} \quad (9),$$

where c is the light speed, ΔE is the total shift of the resonance energy of the coupled microcavities due to the thickness gradient, and d_{tot} is the total thickness. $\Delta E/d_{tot}$ can be interpreted as the optical analogy of the electric field. Since the gradient in thickness, Λ is the average period of the DBR. $\Lambda/d_{tot} \approx N$, number of spacer layers or coupled microcavities. Hence eq. 9 can be further simplified to:

$$\tau = \frac{N}{c\Delta E} \quad (10),$$

For the proposed structure $N = 10$ and $\Delta E = 1400 \text{ cm}^{-1}$ (the relative drift of the resonance is 20% and the microcavity resonance is 7000 cm^{-1}), thus $\tau = 240 \text{ fs}$, which is a good estimation for the simulated PBO period of 260 fs.

7. CONCLUSIONS

The possibility to tune the refractive index of PS multilayers allows the realization of 1D photonic structures, where the photons can be trapped or bounce back and forth. The addition of Er permits to access the interesting wavelength region of 1.55 μm . Two research lines are worth a more detailed study: the propagation of photons in complex 1D photonic structures where extended, critical and localized photon modes coexist; and the search for photonic Bloch oscillations in the time domain for which we proposed a structure based on PS. Unfortunately we had only a short interaction with Giovanna [36] but this was so stimulating that it is at the basis of the proposal to observe the photonic Bloch oscillations we are doing. We are sure that she will be interested in the evolution of our project along these lines.

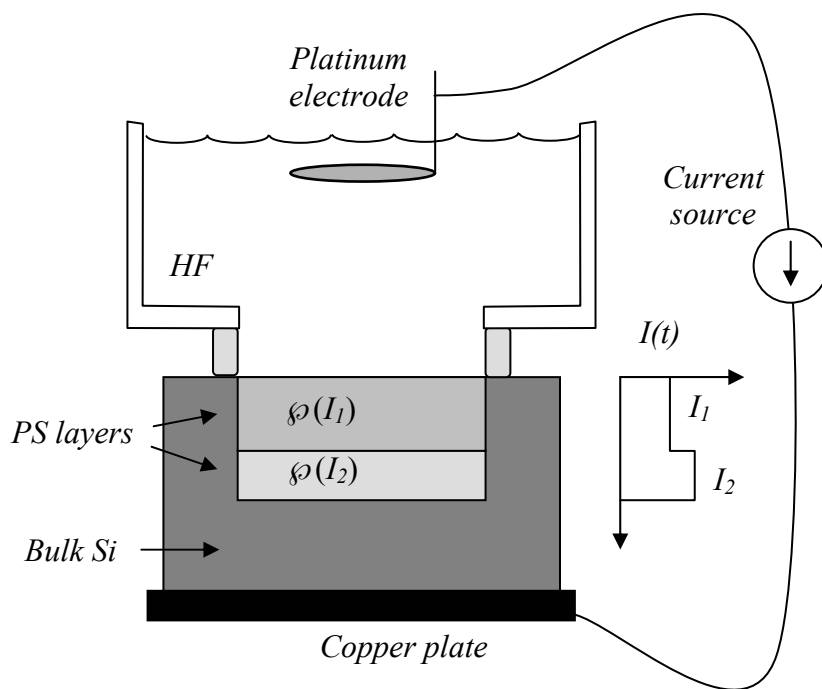
ACKNOWLEDGMENTS

This work was partially supported by INFN through the projects RANDLAS and SMOG. Fruitful discussions with L. C. Andreani, D. S. Wiersma and F. Rossi are acknowledged.

REFERENCES

- 1 Joannopoulos J. D., Meade R. D., and Winn J. N., in *Photonic Crystals* (Princeton University Press, 1995).
- 2 Beale M. I. J., Benjamin J. D., Uren M. J., Chew N. G. and Cullis A. G., *J. Cryst. Growth* **73**, (1985) 622.
- 3 Bisi O., Ossicini S. and Pavesi L., *Surf. Sci. Rep.* **264**, (2000).
- 4 Pavesi L., *Riv. Nuovo Cim.* **10**, (1997).
- 5 Theiß W., *Surf. Sci. Rep.* **29** (3/4) (1997) 91.
- 6 Berger M. G., Arens-Fischer R., Thönissen M., Krüger M., Billat S., Lüth H., Hilbrich S., Theiß W., Grosse P., *Thin Solid Films* **297** (1997) 237.
- 7 Pedrotti F. L. and Pedrotti L. S., *Introduction to Optics* (Prentice-Hall, 1987).
- 8 Bendickson J. M., Dowling J. P. and Scalora M., *Phys. Rev. E* **53**, (1996) 4107.
- 9 Kavokin A., Malpuech G., Di Carlo A., Lugli P. and Rossi F., *Phys. Rev. B* **61** (7), (2000) 4413.
- 10 Pavesi L., Mazzoleni C., Tredicucci A. and Pellegrini V., *Appl. Phys. Lett.* **67** (22) (1995) 3280.
- 11 D'Aguanno G., Centini M., Scalora M., Sibilìa C., Bloemer M. J., Bowden C. M, Haus J. W., and Bertolotti M., *Phys. Rev. E* **63**, (2001) 036610.
- 12 Kimura T., Yokoi A., Horiguchi H., Saito R., Ikoma T. and Sato A., *Appl. Phys. Lett.* **65** (8) (1994) 983.
- 13 Lopez H. A. and Fauchet P., *Appl. Phys. Lett.* **77** (23) (2000) 3704.
- 14 Rammal R., Toulouse G., *J. Phys. Lett.*, **44**, (1983) 412.
- 15 Kohmoto M., Sutherland B., *Phys. Rev. B*, **35**, (1987) 1020.
- 16 Gellermann W., Kohmoto M., Sutherland B. and Taylor P.C., *Phys. Rev. Lett.* **72**, (1994) 633.
- 17 Fujita N., Niizeki K., *Phys. Rev. B* **64**, (2001) 144207.
- 18 Sibilìa C., Tropea F., Bertolotti M., *J. Mod. Opt.*, **45**, (1998) 2255
- 19 Sibilìa C., Nefedov I., Scalora M., Bertolotti M., *JOSA B* **15**, (1998) 1947.
- 20 Sibilìa C., in *Nanoscale linear and nonlinear optics*, edited by M.Bertolotti, C.M.Bowden, C.Sibilìa, AIP conference proceedings **560**, (2000) 220.
- 21 Bertolotti M., Masciulli P., Ranieri P., Sibilìa C., *JOSA B* **13**, (1996) 1512.

- 22 Scalora M., Dowling J.P., Bowden C.M., Bloemer M., *Phys. Rev. Lett.* **73**, (1994) 136.
- 23 Capaz R.B., Koiller B., Queiroz S.L.A., *Phys. Rev. B*, **42**, (1990) 6402.
- 24 Dulea M., Johansson M., Riklund R., *Phys. Rev. B*, **45**, (1992) 105.
- 25 Peng R.W., Wang M., Hu A., Jiang S.S., Gin G.J. and Feng D., *Phys. Rev. B*, **57**, (1998) 1544.
- 26 Gaburro Z., Oton C. J., Bettotti P., Dal Negro L., Vijaya Prakash G., Cazzanelli M. and Pavesi L., submitted to *J. Electrochem. Soc.*
- 27 Macià E., *Phys. Rev. B*, **60** (1999) 10032.
- 28 Oton C. J., Dal Negro L., Gaburro Z., Pavesi L., Johnson P. J., Lagendijk A. and Wiersma D. S., submitted to *Phys. Stat. Sol. A*.
- 29 Rossi F., *Semicond. Sci. Tech.* **13**, (1998) 147.
- 30 Bloch F., *Z. Phys.* **52**, (1928) 555.
- 31 Feldmann J., Leo K., Shah J., Miller D. A. B., Cunningham J. E., Meier T., von Plessen G., Schulze A., Thomas P. and Schmitt-Rink S., *Phys. Rev. B* **46**, (1992) 7252.
- 32 Peschel U., Pertsch T. and Lederer F., *Opt. Lett.* **23** (21), (1998) 1701.
- 33 Lenz G., Talanina I. and Martijn de Sterke C., *Phys. Rev. Lett.* **83** (5) (1999) 963.
- 34 Pertsch T., Dannberg P., Elflein W., Bräuer A., Lederer F., *Phys. Rev. Lett.* **83** (23) (1999) 4752.
- 35 Malpuech G., Kavokin A., Panzarini G. and Di Carlo A., *Phys. Rev. B* **63** (2001) 035108.
- 36 Pavesi L., Panzarini G. and Andreani L. C., *Phys. Rev. B* **58** (1998), 15794.



bitmap version:

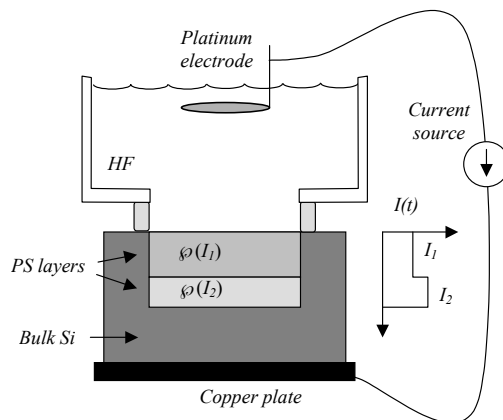


Figure 1: Experimental setup for the fabrication of PS samples. The diagram shows the procedure to grow a two-layer structure. The anodic current is modified and the porosity of the layer changes consequently.

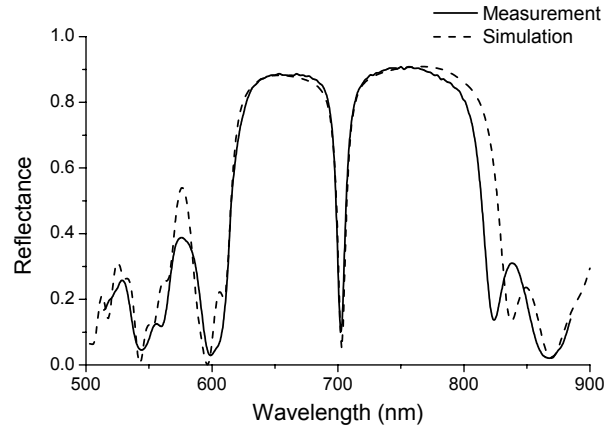


Figure 2: Comparison between a measured (solid line) and a simulated (dashed line) reflectance spectrum of a microcavity tuned at 700 nm sandwiched between two 6-period DBR. The substrate is p⁺-type Si ($\rho = 0.01 \Omega \text{ cm}$), the electrolyte a 1:2 volumetric ratio mixture of aqueous 48% wt. HF and ethanol. The DBRs are made alternating the current between 50 and 5.75 mA/cm² with etch times of 5.04 and 17.45 s. respectively. The central layer is made with 50 mA/cm² for 10.08 s.

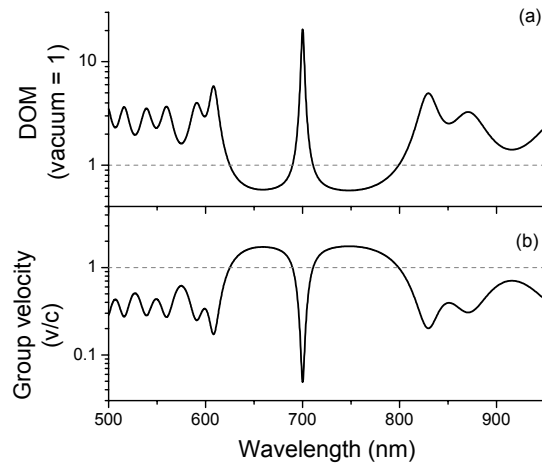


Figure 3: Simulations of the density of optical modes (a) and the group velocity (b) of the microcavity shown in fig. 2.

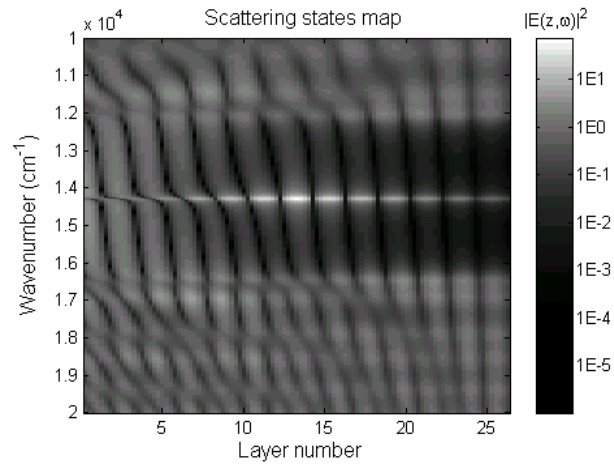


Figure 4: Scattering states map of the microcavity shown in fig. 2, illuminated by white light from the left. The intensity of the white light was normalized to 1.

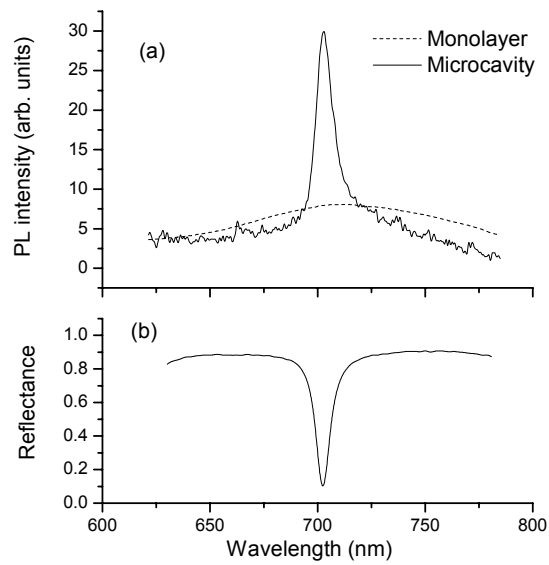


Figure 5: (a) Measured photoluminescence of a monolayer (dashed line) and the microcavity shown in fig. 2. The curves are normalized to have the same area. (b) Measured reflectance spectrum of the microcavity.

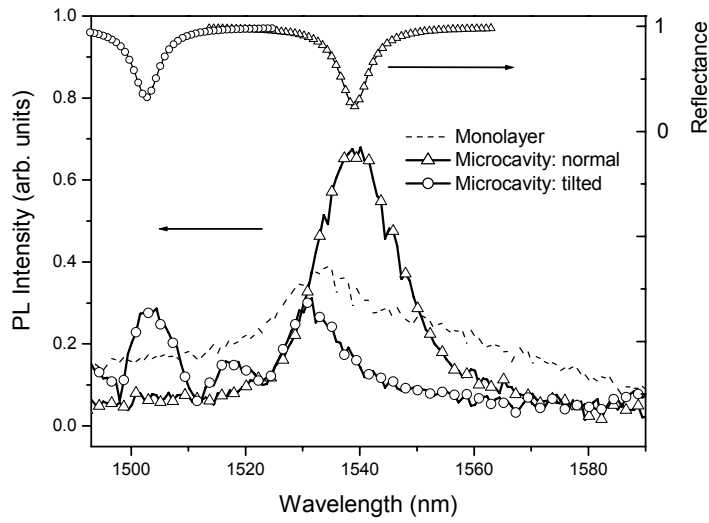


Figure 6: Measured photoluminescence (left axis) of a PS Er-doped monolayer (dashed line), PL spectrum of an Er-doped PS microcavity with normal collecting angle (triangles) and with 23° collecting angle (circles). The parameters of fabrication of the microcavity are the same as in fig. 2 except for the etch times, which are 10.4 and 36.0 for the DBR, and 20.8 s the central layer. The simulations of normal angle and 23° angle reflectances are shown at the top (right axis).

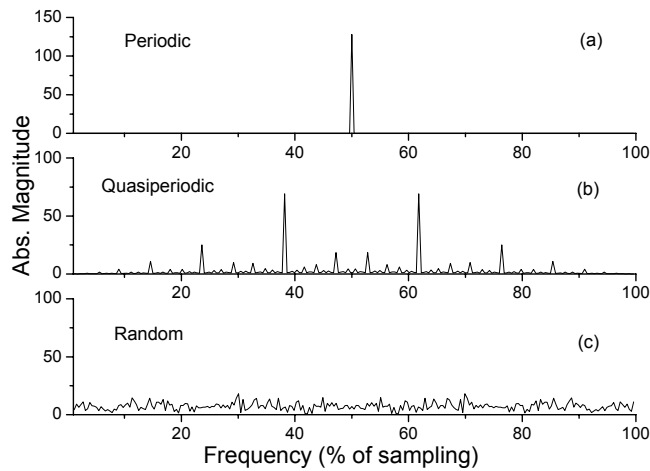


Figure 7: Fourier spectra of different two-component substitutional sequences: (a) a 256-layer periodic sequence obtained by alternating two different building-block layers, (b) a 233-layer Fibonacci sequence and (c) a random two-component sequence.

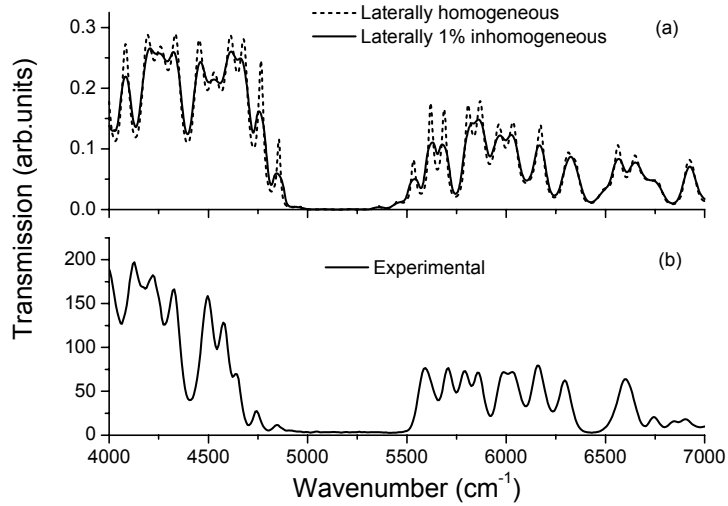


Figure 8: Simulated (a) and measured (b) transmission spectra of a 233 layers PS Fibonacci quasicrystal. A linear drift in the layer parameters has been included in the simulations. The dashed line corresponds to a laterally homogeneous sample and the solid line takes into account a 1% of lateral inhomogeneity.

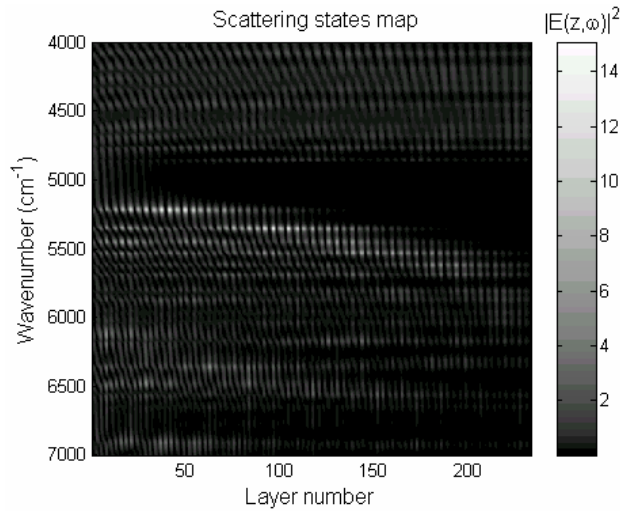


Figure 9: Scattering states map calculation of the 233-layer PS Fibonacci quasicrystal, illuminated with white light from the left. The white light intensity was normalized to 1. Thickness and porosity linear drifts are included in the simulation.

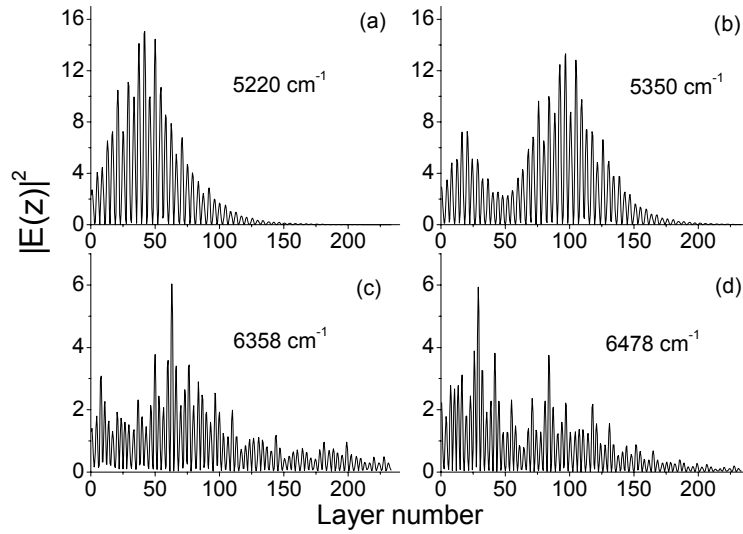


Figure 10: Intensity distribution of the electric fields of (a) the first band-edge resonance, (b) the second band-edge resonance, (c) and (d) two weakly localized modes with field enhancement far away from the Fibonacci band-gap. The input fields are normalized to unity.

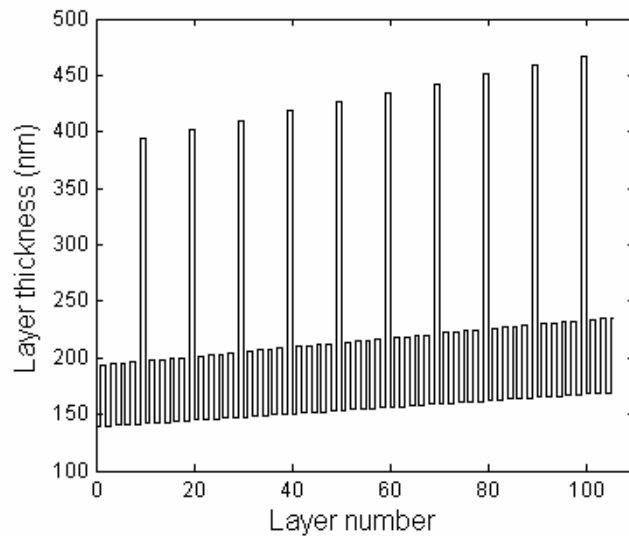


Figure 11: Layer thicknesses of the 10-microcavity structure plus 20% gradient.

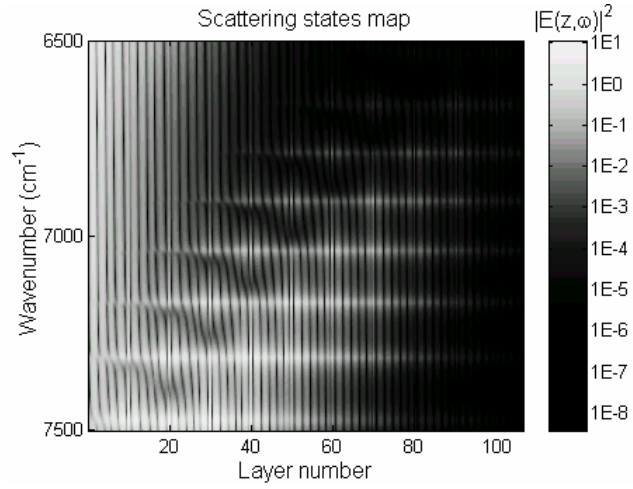


Figure 12: Scattering states map of the structure shown in fig. 11, illuminated by white light on the left. The white light intensity was normalized to 1.. The localized states form a so-called Wannier-Stark ladder (WSL).

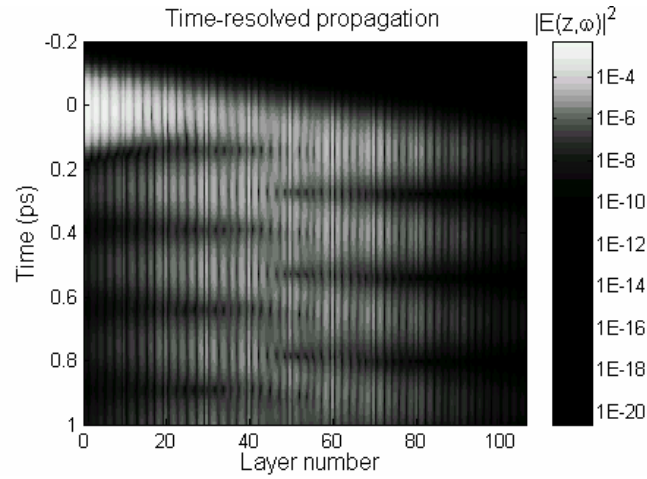


Figure 13: Propagation of an ultrashort laser pulse across the WSL sample. The incoming pulse is centered at 6970 cm^{-1} and its FWHM is 100 cm^{-1} . The oscillations are the so-called photonic Bloch oscillations (PBO).

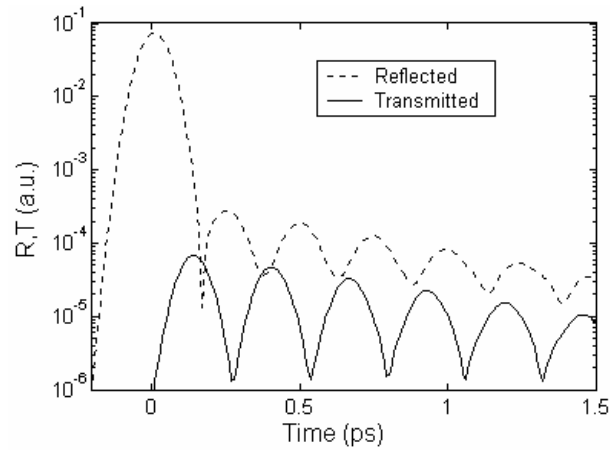


Figure 14: Time-resolved reflectance and transmittance of the pulse simulated in fig. 13. PBO are observable in both signals with a period of 260 fs.

